A Novel Accurate Primary Side Control (PSC) Method for Half-Bridge (HB) LLC Converter

Jae-Bum Lee, Chong-Eun Kim, Jae-Hyun Kim, Cheol-O Yeon, Young-Do Kim, and Gun-Woo Moon
E-mail: leejb83@angel.kaist.ac.kr

***Abstract*—Until now, several researches have been progressed on the primary side control (PSC) methods which decrease the size and cost of the overall system. However, all of them have been applied to the flyback converter, and it is difficult to apply them to the half-bridge (HB) LLC converter due to the large voltage across the secondary leakage inductor of the transformer. In this letter, a new PSC method for the HB LLC converter is proposed to obtain accurate output voltage. In the proposed method, the output voltage is regulated by obtaining the voltage across the primary side of the transformer when the external resonant inductor voltage becomes 0V. At this time, since the voltage across the transformer secondary leakage inductor is small, the proposed method can accurately regulate the output voltage. A 400V input and 20V/85W output laboratory prototype is built and tested to verify the effectiveness of the proposed PSC method.**

Keywords*—Half-bridge (HB) LLC converter, high-power adaptor applications, primary side control (PSC).

I. INTRODUCTION

Recently, as the portable data-processing equipment such as the mobile phones, tablet PCs, and laptop computers has grown explosively and their energy consumption has also been increased, the energy saving has been an essential issue. Meanwhile, since the consumers tend to prefer a compact device, the manufacturers have an effort to minimize its size. For these reasons, the power systems for those devices have been required to be small and achieve a high efficiency. Among the power systems, the adaptors for the laptop computers are strongly required to have a high power density in excess of 5W/in^3 and average efficiency above 85% because of the energy efficiency standards like the energy star program.

At a high power level above 70W for the laptop computers, the conventional adaptors have been developed based on two-stage structure to comply with the IEC 1000-3-2 harmonic standards and obtain a high efficiency [1], [2]. This two-stage configuration consists of the power factor correction (PFC) stage and dc/dc stage. Since the boost converter has many advantages such as a direct control of the line current and low input current ripple, it has been widely utilized in the PFC stage [3], [4]. For the dc/dc stage, the conventional half-bridge (HB) LLC converter is the most attractive candidate because of low voltage stresses on the primary switches and no transformer dc-offset current [5]-[7]. In addition, since it is generally designed in resonant or below region to achieve a full zero-voltage-switching (ZVS) of the primary switches and minimize the switch turn-off losses, it can operate at a high switching frequency, which enables the size of reactive components to be decreased [8]. Due to these many advantages such as a high power density and efficiency, the HB LLC converter has been widely used in the dc/dc stage for high-power adaptor applications.

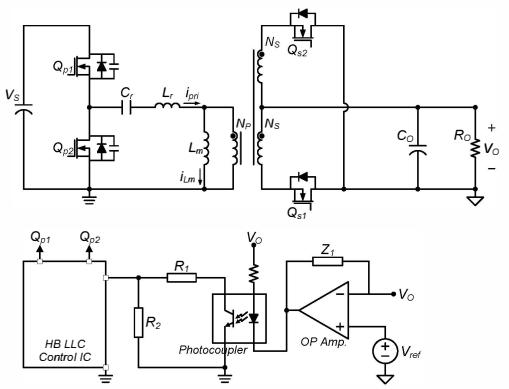

Fig. 1. Schematic of HB LLC converter with conventional SSC method.

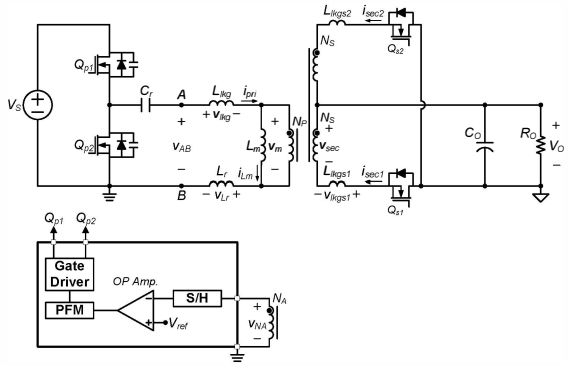

(a) Simplified block diagram.

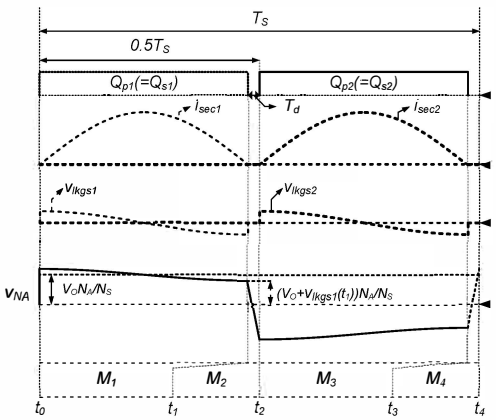

(b) Operational key waveforms.

Fig. 2. Conventional PSC method for HB LLC Converter.

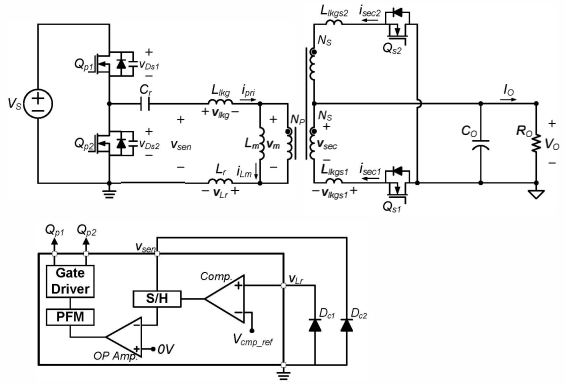

Fig. 3. Block diagram of HB LLC converter with PSC method.

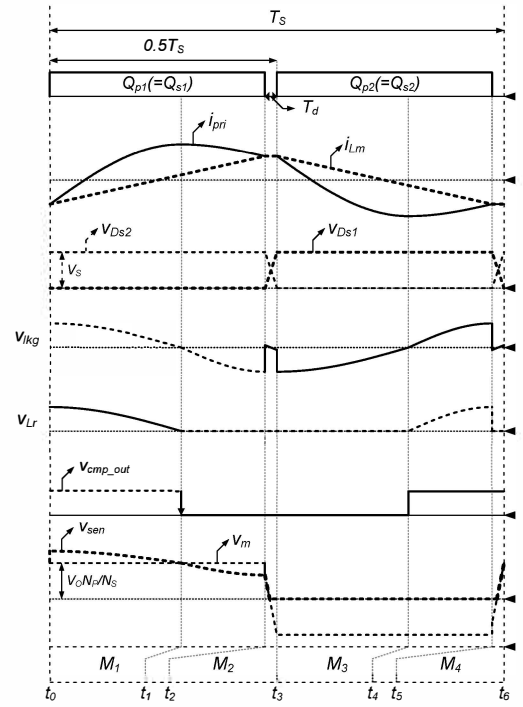

Fig. 4. Key waveforms of HB LLC converter with PSC method.

The HB LLC converter is generally implemented by the secondary side control (SSC), using a HB LLC controller in the primary side, operational amplifier in the secondary side, and photocoupler in between the primary and secondary side to obtain a constant output voltage as shown in Fig. 1. However, since the SSC method requires three ICs with different grounds, it is difficult to integrate them into a single-chip, which increases the size and cost of the overall system. Moreover, the current transfer ratio (CTR) of the photocoupler often changes with the temperature, which degrades the reliability on the control [9], [10].

To overcome the problems of the SSC method, several researches on the primary side control (PSC) method have been proceeded [9]-[14]. By eliminating the photocoupler and secondary feedback circuitry, PSC methods can decrease the size and cost of the overall system compared with the SSC method. However, all of them have been applied only to the flyback converter, and it is difficult to apply them to the HB LLC converter. The reason is stated below. Fig. 2(a) and 2(b) show the simplified block diagram and operational key waveforms of the HB LLC converter with the conventional PSC methods, respectively. In the conventional PSC methods, when the secondary current $i_{sec1}(t)$ reaches 0A at time t_1, the auxiliary winding voltage $v_{NA}(t_1)$ is obtained by the sample-and-hold (S/H) circuit, and the voltage control loop enables $v_{NA}(t_1)$ to follow a reference value V_{ref}. At time t_1 when the primary and secondary switches Q_{p1} and Q_{s1} are turned off, the voltage $v_{sec}(t_1)$ across the secondary side of the transformer and $v_{NA}(t_1)$ become $V_O+v_{lkgs1}(t_1)$ and $N_A(V_O+v_{lkgs1}(t_1))/N_S$, respectively. However, in the HB LLC converter, the voltage $v_{lkgs1}(t_1)$ across the transformer secondary leakage inductor L_{lkgs1} becomes large due to steep slope of $i_{sec1}(t)$ at time t_1 caused by sinusoidal secondary current as shown in Fig. 2(b). Since $v_{NA}(t_1)$ follows V_{ref}, i.e., $V_{ref}=N_A V_O/N_S$, the output voltage cannot be accurately regulated. Therefore, it is difficult to apply the conventional PSC methods to the HB LLC converter due to large $v_{lkgs1}(t_1)$.

In this letter, a new PSC method for the HB LLC converter is proposed as shown in Fig. 3. In the proposed PSC method, the output voltage is regulated by obtaining $v_{sen}(t)$ when the external resonant inductor voltage $v_{Lr}(t)$ becomes 0V. At this time, since the voltage across the transformer secondary leakage inductor is small, the proposed method can accurately regulate the output voltage.

II. PROPOSED METHOD

A. Principle of Proposed PSC Method

Fig. 3 and 4 respectively show the simplified block diagram and operational key waveforms of the HB LLC converter with the proposed PSC method under the following assumptions.

1) All parasitic components except for those specified in Fig. 3 are ignored.
2) The transformer secondary leakage inductors L_{lkgs1} and L_{lkgs2} are ignored. The analysis including L_{lkgs1} and L_{lkgs2} is discussed in Section II-C.
3) The drain-source on-state resistance $R_{ds,on}$ of the secondary switches Q_{s1} and Q_{s2} is small enough to be ignored.
4) The output voltage V_O is constant.

As shown in Fig. 3, the external resonant inductor L_r is located beside the primary ground to easily sense $v_{Lr}(t)$, and two schottky diodes D_{c1} and D_{c2} are used to enable two sensing voltages $v_{Lr}(t)$ and $v_{sen}(t)$ to have positive value that is appropriate for the controller IC. As shown in Fig. 4, the HB LLC converter is regulated by the pulse-frequency modulation (PFM) with a 50% fixed duty cycle, and its operation can be divided into two half cycles t_0–t_3 and t_3–t_6. Since two half cycles have symmetric operation, the first half cycle is only explained.

Mode 1 [t_0–t_2]: The primary switch Q_{p1} is turned on at time t_0. Since the secondary switch Q_{s1} is turned on, the magnetizing inductor current $i_{Lm}(t)$ is linearly increased with a slope of $N_P V_O/N_S/L_m$, and the transformer leakage inductor L_{lkg}, external resonant inductor L_r, and resonant capacitor C_r begin to resonate. Thus, the primary current

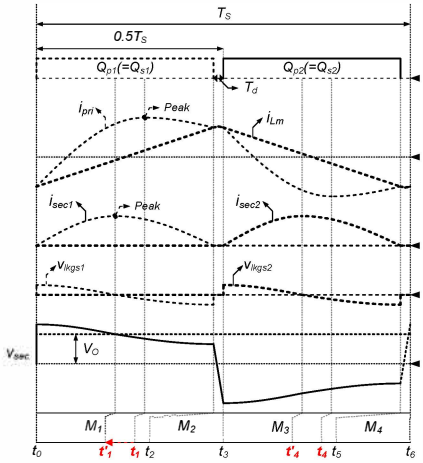

(a) Small L_m.

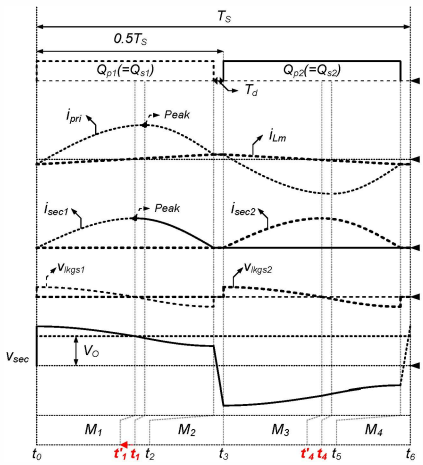

(b) Large L_m.

Fig. 5. The current and voltage waveforms according to L_m.

$i_{pri}(t)$ has sinusoidal shape. The voltages $v_{lkg}(t)$ and $v_{Lr}(t)$ across L_{lkg} and L_r can be expressed as follows:

$$v_{lkg}(t) = L_{lkg}\frac{di_{pri}(t)}{dt} \tag{1}$$

$$v_{Lr}(t) = L_r\frac{di_{pri}(t)}{dt}. \tag{2}$$

Based on (1) and (2), it can be seen from Fig. 4 that $v_{lkg}(t_1)$ and $v_{Lr}(t_1)$ become 0V when $i_{pri}(t)$ reaches its peak value at time t_1. Since $v_{lkg}(t_1)$ and $v_{Lr}(t_1)$ become 0V, $v_{sen}(t_1)$ becomes N_PV_O/N_S. By using the S/H circuit, $v_{sen}(t_1)$ can be obtained, and the voltage control loop enables $v_{sen}(t_1)$ to follow V_{ref}, i.e., V_{ref}=N_PV_O/N_S. Therefore, the output voltage can be accurately regulated by obtaining $v_{sen}(t_1)$ since $v_{lkg}(t_1)$ and $v_{Lr}(t_1)$ become 0V. Due to D_{c1} and D_{c2}, $v_{Lr}(t)$ and $v_{sen}(t)$ below 0V are clamped to 0V.

Mode 2 [t_2–t_3]: At time t_2, $i_{pri}(t)$ becomes equal to $i_{Lm}(t)$, and Q_{p1} is turned off. The peak magnetizing inductor current $i_{Lm}(t_2)$, considered as a current source, discharges the output capacitor of Q_{p2}. Thus, $v_{Ds2}(t)$ is linearly decreased and reaches zero. At this time, Q_{p2} is turned on, and the ZVS of Q_{p2} can be achieved.

B. Implementation of Proposed PSC Method

As mentioned in Section II-A, since $v_{lkg}(t_1)$ and $v_{Lr}(t_1)$ become 0V, $v_{sen}(t_1)$ only includes the information about the output voltage. Therefore, $v_{sen}(t_1)$ should be obtained by detecting the point that $v_{Lr}(t)$ becomes 0V. As shown in Fig. 4, $v_{Lr}(t)$ is compared with 0V. When $v_{Lr}(t)$ decreases and reaches 0V at time t_1, the output $v_{cmp\_out}(t_1)$ of the comparator is changed from high value to low value. By using the S/H circuit, $v_{sen}(t_1)$ can be obtained at only falling edge of $v_{cmp\_out}(t)$ [12]. Based on the simplified block diagram in Fig. 3, the proposed method can be a single-chip solution.

C. Effect of Transformer Secondary Leakage Inductor

In this section, since the transformer secondary leakage inductors L_{lkgs1} and L_{lkgs2} have a strong influence on the regulation accuracy, the analysis considering L_{lkgs1} and L_{lkgs2} is discussed. Fig. 5(a) and 5(b) show the current and voltage waveforms according to L_m, considering L_{lkgs1} and L_{lkgs2}. During mode 1, $i_{Lm}(t)$ is linearly increased with a slope of $N_PV_O/N_S/L_m$, and L_{lkg}, L_r and C_r resonate. Therefore, $i_{Lm}(t)$ and $i_{pri}(t)$ can be expressed as follows:

$$i_{Lm}(t) = \frac{N_PV_O}{N_SL_m}(t-t_0) - \frac{N_PV_O}{4N_SL_mF_S} \tag{3}$$

$$i_{pri}(t) = i_{pri}(t_0)\cos\left(\omega_O(t-t_0)\right) + \left(\frac{V_S - v_{Cr}(t_0) - N_PV_O/N_S}{Z}\right)\sin\left(\omega_O(t-t_0)\right), \tag{4}$$

where $v_{Cr}(t_0)$ and $i_{pri}(t_0)$ are the initial values of the resonant capacitor voltage $v_{Cr}(t)$ and primary current $i_{pri}(t)$, F_S is the switching frequency, and the characteristic impedance Z and resonant angular frequency ω_O are defined as $[(L_{lkg}+L_r)/C_r]^{0.5}$ and $1/[(L_{lkg}+L_r)C_r]^{0.5}$.

Based on (1) and (2), when $i_{pri}(t)$ reaches its peak value at time t_1, both $v_{lkg}(t)$ and $v_{Lr}(t)$ become 0V, and t_1 can be expressed as follows:

$$t_1 = t_0 + \frac{1}{\omega_O}\left[\pi + \tan^{-1}\left(\frac{V_S - v_{Cr}(t_0) - N_PV_O/N_S}{i_{pri}(t_0)Z}\right)\right]. \tag{5}$$

Meanwhile, the secondary current $i_{sec1}(t)$ during mode 1 is the difference between $i_{pri}(t)$ and $i_{Lm}(t)$, and $i_{sec1}(t)$ can be expressed as follows:

$$i_{sec1}(t) = \frac{N_P}{N_S}\left(i_{pri}(t) - i_{Lm}(t)\right). \tag{6}$$

As shown in Fig. 5(a) and 5(b), since $i_{sec1}(t)$ reaches its peak value at time not t_1 but t'_1, the voltage $v_{lkgs1}(t_1)$ across L_{lkgs1} becomes negative, and t'_1 can be expressed as follows:

$$t'_1 = t_1 - \frac{1}{\omega_O}\sin^{-1}\left[\frac{N_PV_O}{N_SL_m\omega_O\sqrt{i_{pri}^2(t_0) + \left(\frac{V_S - v_{Cr}(t_0) - N_PV_O/N_S}{Z}\right)^2}}\right]. \tag{7}$$

From (7), as the transformer magnetizing inductor L_m is decreased, it can be seen from Fig. 5(a) that t'_1 deviates farther from t_1 and $v_{lkgs1}(t_1)$ becomes more negative due to steep slope of $i_{sec1}(t)$ at time t_1. In the proposed method, since $v_{sec}(t_1)$ and $v_{sen}(t_1)$ respectively become V_O+$v_{lkgs1}(t_1)$ and $N_P(V_O$+$v_{lkgs1}(t_1))/N_S$, designing large L_m indicates that $v_{lkgs1}(t_1)$ is small and accurate output voltage is obtained.

Meanwhile, in the HB LLC converter with the conventional PSC methods, when $i_{sec1}(t)$ reaches 0A at

TABLE I
CIRCUIT PARAMETERS OF HB LLC CONVERTER WITH PSC METHODS

Rated power	85W	Input voltage, V_S	400V
		Output voltage, V_O	20V
Main switches (Q_1, Q_2)	IPP60R600CP		
External resonant inductor (L_r)	31.05μH		
Resonant capacitor (C_r)	47nF		
Main transformer	Core	PQ2620	
	$N_P : N_S : N_S = 20 : 2 : 2$ L_m: 2.37mH, L_{lkg}: 5.5μH		
Secondary switches (SR_1, SR_2)	BSC077N12NS3G (120V, 98A, $R_{ds,on}$: 7.7mΩ)		

TABLE II
MEASURED OUTPUT VOLTAGE OF PSC METHODS ACCORDING TO OUTPUT LOAD

Output load	Output Voltage		Output load	Output Voltage	
	Conventional PSC Method	Proposed PSC Method		Conventional PSC Method	Proposed PSC Method
10%	20.135V	20.051V	60%	20.401V	20.110V
20%	20.191V	20.061V	70%	20.454V	20.123V
30%	20.242V	20.072V	80%	20.507V	20.136V
40%	20.294V	20.084V	90%	20.560V	20.148V
50%	20.348V	20.095V	100%	20.614V	20.162V

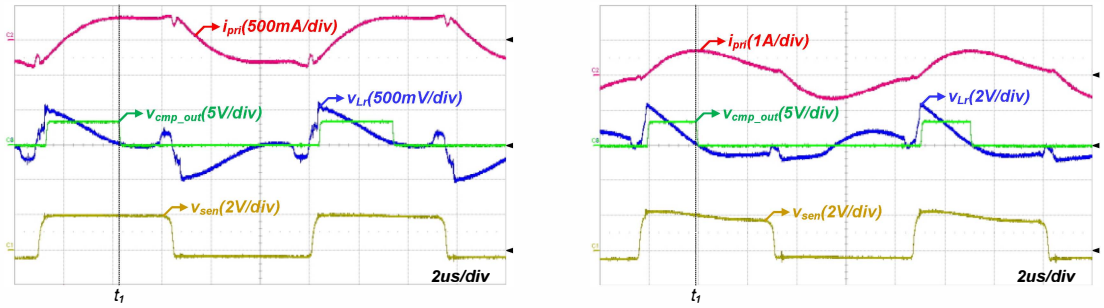

(a) At 10% load conditions. (b) At full load conditions.

Fig. 6. Experimental key waveforms of i_{pri}, v_{Lr}, v_{cmp_out}, and v_{sen} at 10% and full load conditions.

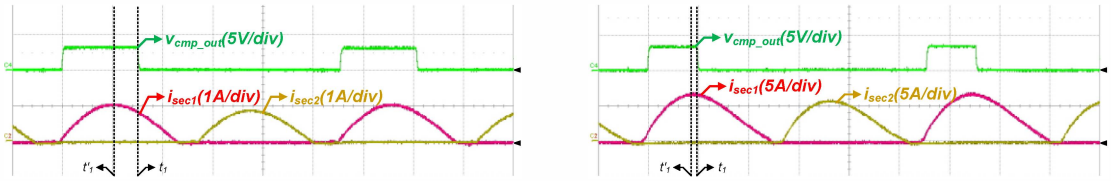

(a) At 10% load conditions. (b) At full load conditions.

Fig. 7. Experimental key waveforms of v_{cmp_out}, i_{sec1}, and i_{sec2} at 10% and full load conditions.

time t_2 as shown in Fig. 5(a) and 5(b), $v_{NA}(t_2)$ is obtained, i.e. $v_{NA}(t_2)=N_A(V_O+v_{lkgs1}(t_2))/N_S$. Since $v_{lkgs1}(t_2)$ is larger than $v_{lkgs1}(t_1)$, the output voltage in the conventional PSC methods can be less accurately regulated than that in the proposed PSC method.

III. EXPERIMENTAL RESULTS

To verify the validity of the proposed PSC method for the HB LLC converter, a 85W prototype converter with the specification of V_S=400V and V_O=20V has been built, and a PIC33FJ16GS502 micro control unit (MCU) is utilized. The design parameters utilized in this experiment are presented in Table I.

Fig. 6(a) and 6(b) show the experimental key waveforms of the HB LLC converter with the proposed PSC method at 10% and full load conditions. As can be seen from $i_{pri}(t)$ and $v_{Lr}(t)$ in Fig. 6(a) and 6(b), $v_{Lr}(t_1)$ becomes 0V when $i_{pri}(t)$ reaches its peak value at time t_1. In addition, from $v_{cmp\_out}(t)$ in Fig. 6(a) and 6(b), it can be seen that $v_{cmp\_out}(t_1)$ is changed from high value to low value. Moreover, from $i_{sec1}(t)$ in Fig. 7(a) and 7(b), it can be seen that $i_{sec1}(t)$ reaches its peak value at time not t_1 but t'_1. However, since L_m is large enough, the slope of $i_{sec1}(t)$ is gradual at time t_1, and $v_{lkgs1}(t_1)$ is small.

Table II shows the measured output voltage of the conventional and proposed PSC methods according to the load conditions. As shown in this table, it can be seen that the proposed method has the improved output voltage regulation capability within 0.81% by minimizing $v_{lkgs1}(t_1)$ compared the output voltage regulation

capability of the conventional method within 3.1%.

IV. CONCLUSIONS

This paper introduces a new PSC method for the HB LLC converter. The proposed method has the output voltage regulation capability within 0.81% by minimizing the voltage across the transformer secondary leakage inductor. The validity of this study is confirmed by the experimental results. It is suitable for high-power adaptor applications employing the HB LLC converter for the tablet PCs and laptop computers.

ACKNOWLEDGMENT

This work was supported by the National Research Foundation of Korea(NRF) grant funded by the Korea government(MSIP) (No.2010-0028680).

REFERENCES

[1] Y. Panov and M. M. Jovanovic, "Performance Evaluation of 70-W Two-Stage Adaptors for Notebook Computers," in *Proc. IEEE APEC*, 1999, pp. 1059-1065.

[2] S. W. Choi, B. W. Ryu, and G. W. Moon, "Two-Stage AC/DC Converter Employing Load-Adaptive Link-Voltage-Adjusting Technique with Load Power Estimator for Notebook Computer Adaptor," in *Proc. IEEE ECCE*, 2009, pp. 3761-3767.

[3] L. H. S. C. Barreto, M. G. Sebastiao, L. C. de Freitas, E. A. Alves Coelho, V. J. Farias, and J. B. Vieira, "Analysis of a Soft-Switched PFC Boost Converter Using Analog and Digital Control Circuits," *IEEE Trans. Ind. Electron.*, vol. 52, no. 1, pp. 221–227, Feb. 2005.

[4] J. P. R. Balestero, F. L. Tofoli, R. C. Fernandes, G. V. Torrico-Bascope, and F. J. M. de Seixas, "Power Factor Correction Boost Converter Based on the Three-State Switching Cell," *IEEE Trans. Ind. Electron.*, vol. 59, no. 3, pp. 1565–1577, Mar. 2012.

[5] B. Yang, F. C. Lee, A. J. Zhang, and G. Huang, "LLC Resonant Converter for Front End DC/DC Conversion," in *Proc. IEEE APEC*, 2002, pp. 1108-1112.

[6] D. Y. Kim, C. E. Kim, and G. W. Moon, "High-Efficiency Slim Adapter With Low-Profile Transformer Structure," *IEEE Trans. Ind. Electron.*, vol. 59, no. 9, pp. 3445–3449, Sep. 2012.

[7] I. O. Lee and G. W. Moon, "The *k*-Q Analysis for an *LLC* Series Resonant Converter," *IEEE Trans. Power Electron.*, vol. 29, no. 1, pp. 13–16, Jan. 2014.

[8] K. Jin, X. Ruan, M. Yang, and M. Xu, "A Hybrid Fuel Cell Power System," *IEEE Trans. Ind. Electron.*, vol. 56, no. 4, pp. 1212–1222, Apr. 2009.

[9] J. Fang, Z. Lu, Z. Li, and Z. Li, "A New Flyback Converter with Primary Side Detection and Peak Current Mode Control," in *Proc. IEEE ICCCAS*, 2002, pp. 1707-1710.

[10] J. Shen and T. Liu, "Constant Current LED Driver Based on Flyback Structure with Primary Side Control," in *Proc. IEEE PEAM*, 2011, pp. 260-263.

[11] X. Xie, J. Wang, C. Zhao, Q. Lu, and S. Liu, "A Novel Output Current Estimation and Regulation Circuit for Primary Side Controlled High Power Factor Single-Stage Flyback LED Driver," *IEEE Trans. Power Electron.*, vol. 27, no. 11, pp. 4602–4612, Nov. 2012.

[12] Jianwen Shao, "A Highly Accurate Constant Voltage (CV) and Constant Current (CC) Primary Side Controller for Offline Applications," in *Proc. IEEE APEC*, 2013, pp. 3311-3316.

[13] H. H. Chou, Y. S. Hwang, and J. J. Chen, "An Adaptive Output Current Estimation Circuit for a Primary-Side Controlled LED Driver," *IEEE Trans. Power Electron.*, vol. 28, no. 10, pp. 4811–4819, Oct. 2013.

[14] Y. C. Li and C. L. Chen, "A Novel Primary-Side Regulation Scheme for Single-Stage High-Power-Factor AC-DC LED Driving Circuit," *IEEE Trans. Ind. Electron.*, vol. 60, no. 11, pp. 4978–4986, Nov. 2013.